Desorption of metal atoms with laser light: Mechanistic studies

W. Hoheisel, M. Vollmer, and F. Träger
Fachbereich Physik, Universität Kassel, Heinrich-Plett-Straße 40, D-34132 Kassel, Germany
(Received 21 December 1992)

Results on laser-induced desorption of metal atoms from small metal particles are presented. Experiments have been performed on sodium, potassium, and silver particles supported on a LiF(100) single-crystal surface under ultrahigh vacuum conditions. Measurements include the determination of the desorption rate as a function of laser wavelength, laser intensity, average particle size, and substrate temperature, the determination of the kinetic energy of the desorbed atoms, the investigation of the optical spectra of the supported metal particles, and the study of the influence of adsorbate molecules on the desorption rate. Furthermore, theoretical extinction and absorption spectra of the metal particles have been calculated with the classical electrodynamical Mie theory as a function of average particle size and excitation wavelength. Also, the radial electric field at the particle surface was computed. The results of the experiments and theoretical calculations are combined to give a consistent picture of the mechanism of metal-atom desorption by electronic excitation with laser light. A realistic surface potential from which the atoms escape and nonlocal optical effects are taken into account. The latter introduce additional absorption channels by the formation of electron-hole pairs in the surface layer of the particle which relax into antibonding states before desorption occurs. Finally, the mechanism is discussed in the light of similar phenomena observed for thin metal films. Possibilities for future work are outlined.

I. INTRODUCTION

If small metal particles[1] are irradiated with visible, continuous-wave laser light, desorption of metal atoms from the surface of these particles can be observed. The principle of such experiments is shown schematically in Fig. 1. In the past, desorption of alkali-metal atoms has been observed and analyzed with the main goal of studying the underlying desorption mechanism.[2–7] In other work, nonthermal desorption of metal atoms has been found to occur also from the surface of thin gold, silver, and aluminum films.[8–11] All of these experiments show that the underlying mechanism is based directly on electronic excitation, and is nonthermal. This is quite surprising, since it was commonly believed that desorption of metal atoms by electronic excitation is difficult to accomplish, if not impossible, because the excitation is usually quenched on such a short time scale that an atom has no chance to escape from the surface potential. Still, the observed laser detachment of different metal atoms indicates that the mechanism is of a very general nature. In view of these arguments, experimental as well as theoretical investigations which further clarify the bond breaking mechanism are highly interesting.

In general, desorption of metal atoms with visible light, i.e., by absorption of photons with energies on the order of several eV, constitutes a special case of a DIET (desorption induced by electronic transitions, see, e.g., Ref. 12) process. In the classical field of DIET, desorption involving inner-shell excitation with fast electrons or highly energetic photons has been studied extensively. Desorption mechanisms, such as the scenarios of Menzel and Gomer,[13] and Readhead,[14] and Knoteck and Feibelman[15] have been developed. Undoubtedly, these models can be helpful to understanding why and how metal atoms desorb. One cannot anticipate, however, that they can readily explain details of the mechanism of metal-atom detachment by relatively low-energy photons. Desorption of atoms with visible light also falls into the

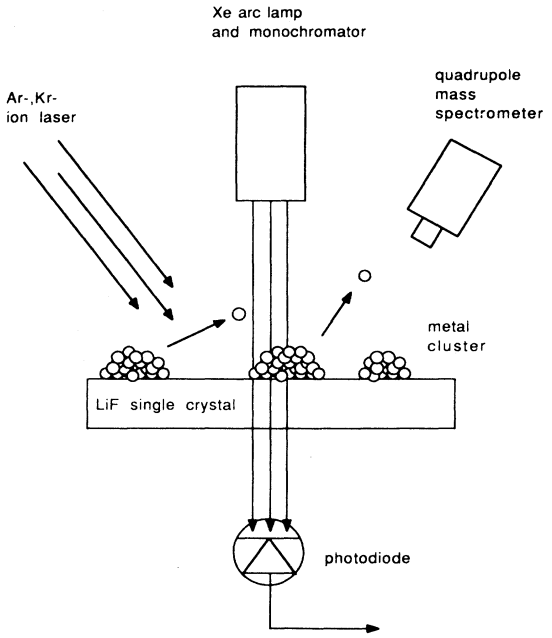

FIG. 1. Schematic representation of an experiment for the study of metal-atom desorption from the surface of small metal particles by electronic excitation with continuous-wave visible laser light. Detection of the atoms is accomplished with a quadrupole mass spectrometer. The Xe arc lamp is used in combination with a monochromator to measure the optical transmission spectra of the metal particles.

category of laser-induced surface processes (see, e.g., Refs. 16–18) that have been studied extensively during the last years.

The present paper reports results of laser-induced desorption of metal atoms from small metal particles. Experiments have been performed on potassium and silver in addition to a continuation of our earlier work on sodium. Metal atoms were desorbed from metal clusters supported on a LiF(100) single-crystal surface under ultrahigh vacuum conditions. Measurements include the determination of the desorption rate as a function of the laser wavelength and intensity, as well as of the particle size and substrate temperature. In addition, the kinetic energy of the desorbed atoms was measured and the optical spectra of the supported metal particles were investigated. Also, different molecules were adsorbed on the surface of the particles in order to study their influence on the desorption process. Furthermore, theoretical calculations of the optical spectra of the metal particles have been performed with the classical Mie theory as a function of average particle size and excitation wavelength. Also, the radial electric field at the particle surface was computed. The results of the experiments and theoretical calculations are combined in a model which gives a consistent picture of the mechanism of metal-atom desorption by electronic excitation with laser light. An essential feature of this model is the consideration of a realistic surface potential and nonlocal optical effects.[19] This concept gives a more precise and physically meaningful description of the interaction of light with the surface layer of the metal particles, as compared to the classical step function often used for the electron-density distribution at the surface. Furthermore, the nonlocal optical effects give rise to new absorption channels in the surface layer by the formation of electron-hole pairs. Quenching of such excitations by coupling to the phonons can be strongly suppressed at surface sites with a low coordination number, making desorption possible. The proposed mechanism is finally discussed in the light of the above-mentioned experiments on thin metal films.

II. EXPERIMENT

A. Setup and sample preparation

The experimental arrangement has been discussed in detail elsewhere.[4] Here only a short description will be given. The experiments were performed in an ultrahigh vacuum system with a base pressure in the low 10^{-10}-mbar range. A LiF(100) single-crystal surface served as the substrate for the metal particles. It was cleaned and annealed by heating, and subsequently cooled to 90 K. A collimated thermal atomic beam was directed onto the substrate, where the impinging metal atoms were captured in the surface potential. The flux of the atomic beam was measured with a quartz-crystal microbalance, and was on the order of $10^{13}\ s^{-1}\,cm^{-2}$. The metal particles were formed by surface diffusion and nucleation. The average size of the clusters could be controlled in a reproducible manner by exposing the surface to the atomic beam for different periods of time. The mean particle size was determined by inelastic scattering of atoms during the deposition,[20] by thermal desorption,[21] and by *in situ* measurement of the optical transmission spectra.[22] The number density of the particles on the surface was 10^8–$10^9\ cm^{-2}$ for alkali clusters, and $10^{10}\ cm^{-2}$ for Ag clusters. The average radii ranged from $R=5$ to 100 nm, depending on the deposition time. Desorption was accomplished by the light of an Ar^+ ion, Kr^+ ion, or continuous-wave tunable dye laser. The beam had a Gaussian profile and a radius of $r_{1/2}=1.0$ mm on the sample surface, $r_{1/2}$ being the radius at which the intensity has dropped to half of the maximum value. Wavelengths ranging from $\lambda=351$ to 752 nm, and light powers between 2 mW and 10 W were used. This corresponds to intensities between 40 mW/cm^2 and 200 W/cm^2. The desorbed atoms were ionized by electron impact, mass selected in a quadrupole filter, and finally detected in a single-ion-counting mode. In several experiments, gases like ND_3 (Ref. 23) and CO were adsorbed on the particle surface, and their influence on the desorption rate was studied. In order to determine the kinetic energy of the atoms, time-of-flight measurements were carried out by chopping the continuous-wave laser beam mechanically with a rotating wheel. This gave light pulses of 2-μs duration at a repetition rate of about 1800 Hz. In several experiments a Nd:YAG (yttrium aluminum garnet) laser with a pulse duration of 10 ns and a wavelength of $\lambda=532$ mn was also applied. Pulse energies ranged from 5 μJ to 10 mJ. The optical extinction of the supported clusters was measured as a function of wavelength with a high-pressure Xe arc lamp combined with a grating monochromator. The spectral resolution was chosen to be $\Delta\lambda=3$ nm. As the last step of each experiment, thermal desorption of the metal atoms from the surface was recorded by heating the LiF crystal to $T=700$ K. This served both for cleaning of the sample and for an additional determination of the absolute coverage of metal atoms.

B. Desorption rate measurements

The desorption rate was measured under continuous-wave laser irradiation as a function of light intensity, wavelength, average particle size, and temperature. Sodium, potassium, and silver particles were studied. For Na and K, desorption can be readily detected at a rate of typically 1000 counts per second if the laser power is on the order of 1 W [see Figs. 2(a) and 2(b)]. Taking the solid angle under which the atoms reach the electron impact ionizer and the detection sensitivity of the quadrupole mass spectrometer into account, this corresponds to about 10^{12} desorbed atoms per second. In contrast to Na and K, laser-induced desorption of Ag atoms exhibits a burstlike signal [see Fig. 2(c)]. It disappears after several seconds of irradiation time, very likely because only few sites from which atoms can desorb exist on the particle surface. Naturally desorption can only occur if the absorbed photon energy exceeds the binding energy of a surface atom. For Ag, however, the value of the binding energy (in Na and K about $\frac{2}{3}$ of the bulk cohesive energy) of 2.95 eV is ≈ 2 eV and almost equals the absorbed pho-

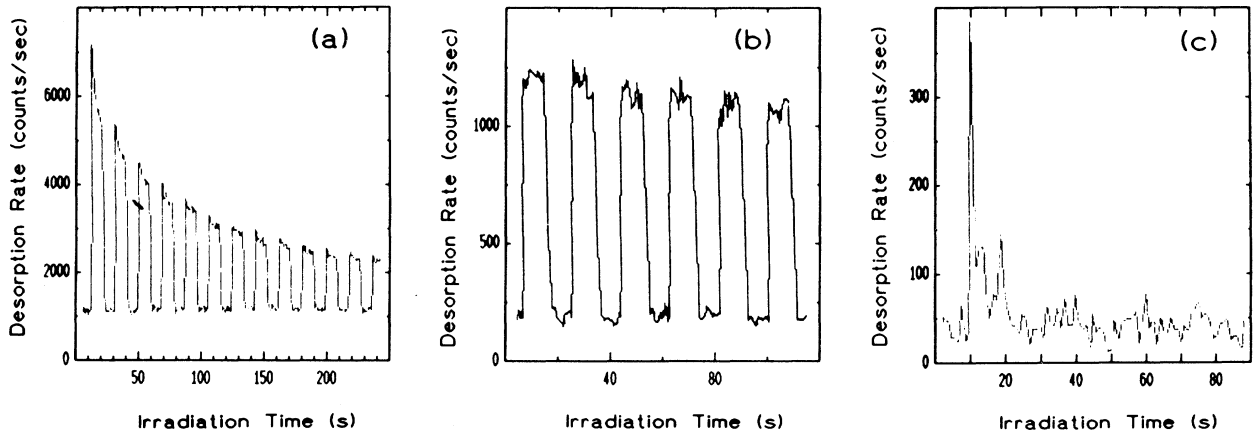

FIG. 2. (a) Desorption rate of Na atoms from the surface of small Na particles under laser irradiation for a number of laser-on–laser-off periods. The mean particle size was 50 nm, the laser power 5 W, and the wavelength 514 nm. (b) Desorption rate of K atoms from the surface of small K particles. The mean particle size was 58 nm, the laser power 3.5 W, and the wavelength 647 nm. (c) Desorption rate of Ag atoms detached from the surface of small Ag particles. The mean particle size was 40 nm, the laser power 10 W, and the laser wavelength 514 nm.

ton energy, being in the range of 2–3.5 eV. It is therefore plausible that the signal disappears as soon as the sites from which atoms with low binding energy can desorb are depleted. Improvements, such as other preparation conditions for the particles, or use of higher temperatures, should make possible the larger desorption rate needed for systematic investigations of Ag in the future.

For all metals investigated, the desorption rate rises immediately if the laser beam is incident on the particles, and stops promptly if the light beam is blocked. The temporal dependence of the desorption rate can be very different: it can decrease as a function of time, as shown in Fig. 2, but also exhibits an increase followed by a maximum and then gradually drops off. This behavior is discussed in detail elsewhere, and results from the choice of different particle size distributions at a given laser wavelength.[24]

At fixed light intensity and fixed mean particle radius, the desorption rate depends resonantly on the excitation wavelength (see Fig. 3). Also, the desorption signal shows a resonant dependence on the mean cluster radius if the laser wavelength is kept constant (see Fig. 4). For even larger particles with $R > 60$ nm the desorption rate drops off further and further[3] until the signal finally ($R > 150$ nm) approaches the noise level. This observation is of particular importance for the interpretation of the desorption mechanism discussed below. For very small particles with $R < 5$ nm the desorption rate increases with the third power, and for particles with $5 < R < 10$ nm with the second power of the average radius (see Fig. 5). As an additional example of the desorption rate measurements, Fig. 6 displays the rate of potassium atoms as a function of the mean particle radius for different excitation wavelengths of the laser light.

The rate of desorbed atoms increases linearly as a function of light intensity over the entire available power range,[3] i.e., over nearly four orders of magnitude (see Fig. 7). This linear behavior is independent of wavelength. In the case of sodium the quantum efficiency of the process is on the order of 10^{-4} at the maximum of the resonance, i.e., one metal atom is desorbed per 10 000 absorbed photons. The desorption rate dn/dt depends exponentially on the particle temperature (see Fig. 8). A fit of the experimental data to the exponential dependence $dn/dt \sim \exp[-E/kT]$ gives an activation energy of $E = 0.14$ eV.

Another interesting behavior of the desorption rate appears if the metal particles are covered by adsorbate molecules such as deuterated ammonia (ND_3) or carbon monoxide (CO). The desorption rate of metal atoms decreases as compared to the clean particle surface, but the

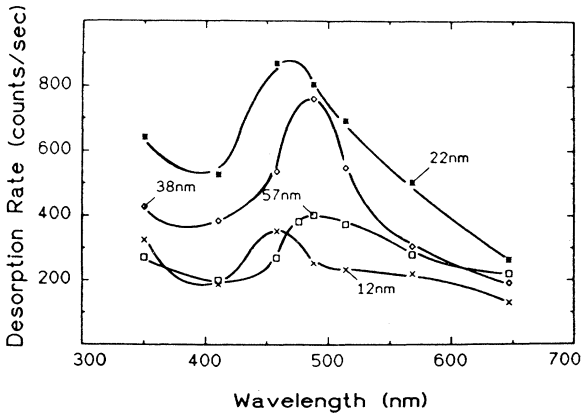

FIG. 3. Desorption rate of Na atoms detached from the surface of small Na particles as a function of wavelength for different particle sizes.

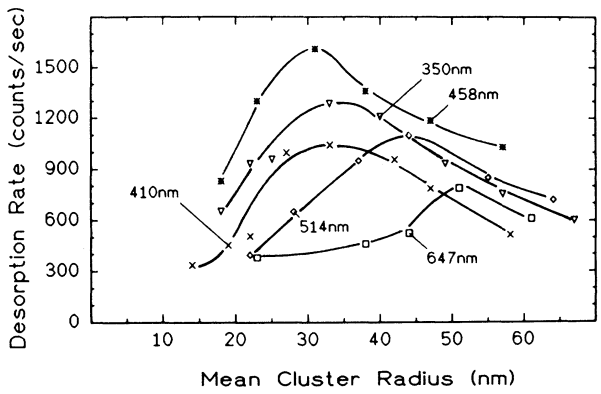

FIG. 4. Desorption rate of Na atoms detached from the surface of small Na particles as a function of mean particle radius for different excitation wavelengths.

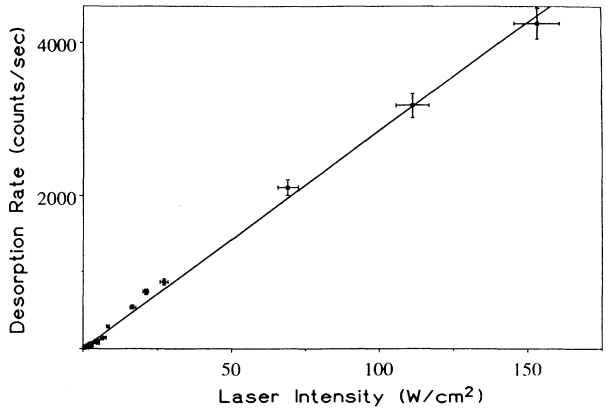

FIG. 7. Desorption rate of Na atoms desorbed from the surface of small Na particles as a function of laser intensity. The linear behavior of the desorption rate could be established down to an intensity of 40 mW/cm^2. No threshold was observed.

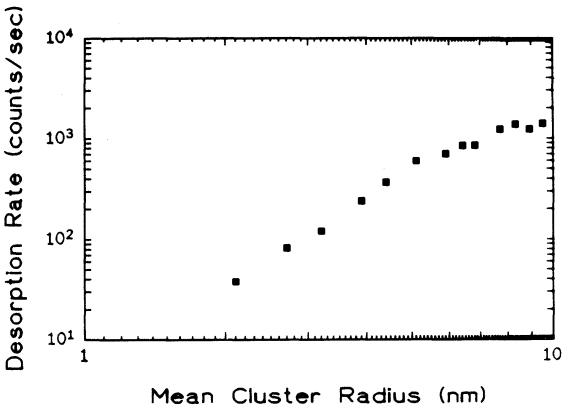

FIG. 5. Desorption rate of Na atoms detached from the surface of small Na particles as a function of average particle radius with $R < 10$ nm. The laser wavelength was $\lambda = 514$ nm.

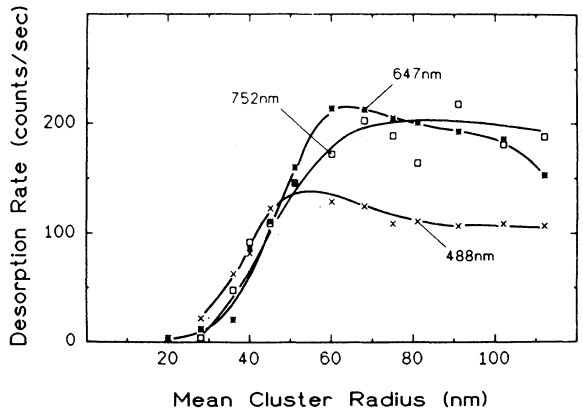

FIG. 6. Desorption rate of K atoms desorbed from the surface of small K particles as a function of the mean particle radius for different excitation wavelengths of the laser light.

time dependence of the signal remains unchanged (see Fig. 9). The desorption rate of the adsorbed molecules, however, shows a *slow increase* if the laser illuminates the sample, and a *gradual decrease* after the light beam is blocked. Furthermore, desorption also takes place during the laser-off periods. Both are typical of a thermal process; thermal desorption of the same sample without laser irradiation indicates that the ND_3 molecules already desorb at a very small temperature rise. Thermal evaporation of the Na particles, on the other hand, does not occur before a temperature of $T = 300$ K has been reached.[21] Actually, desorption of molecules like ND_3 provides an elegant means to estimate an upper limit for the surface temperature rise of the metal particles as a result of the absorption of laser light. Among other observations,[3] the immediate rise and decay of the rate of metal atoms as compared to the slow response of the ND_3 signal indicates the nonthermal nature of the mechanism underlying the desorption of metal atoms.

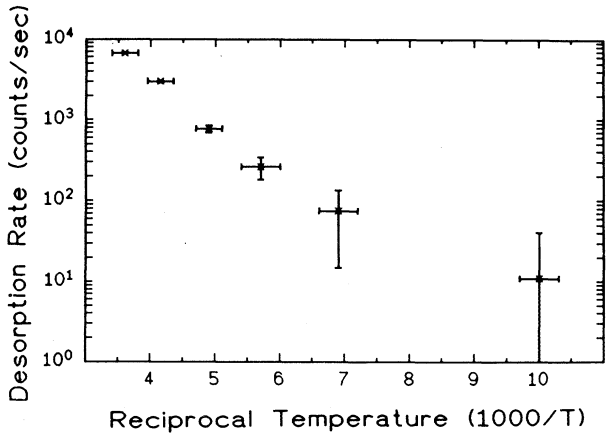

FIG. 8. Laser-induced desorption rate of Na atoms as a function of the inverse of the substrate temperature for a fixed mean particle radius of 50 nm, laser power of 7 W, and wavelength of 514 nm.

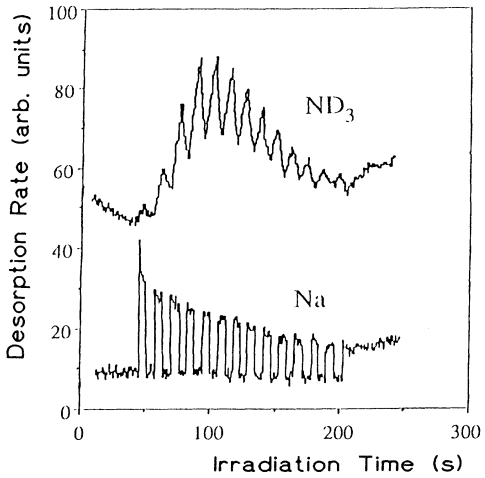

FIG. 9. Laser-induced desorption rate (arbitrary units) of Na atoms and ND_3 molecules from the surface of small Na particles covered with approximately one monolayer of ND_3. The ND_3 rate is displayed with an offset. From the different transient behavior of the desorption rates it can be seen clearly that the Na atoms desorb by a nonthermal mechanism, whereas the ND_3 molecules are detached by thermal desorption.

C. Kinetic-energy measurements

The kinetic energy of the desorbed metal atoms was determined by time-of-flight measurements. Figure 10 and 11 show examples of time-of-flight spectra for Na and K, respectively. For a correct determination of the kinetic energy, the time period between electron impact ionization and ion detection by the multiplier of the mass spectrometer was subtracted from the measured flight times. This average drift time of the ions in the detection system was measured with three independent methods, and is 18 μs for Na, and 22 μs for K.[25] As can be seen from Figs. 10 and 11, the time-of-flight spectra show a

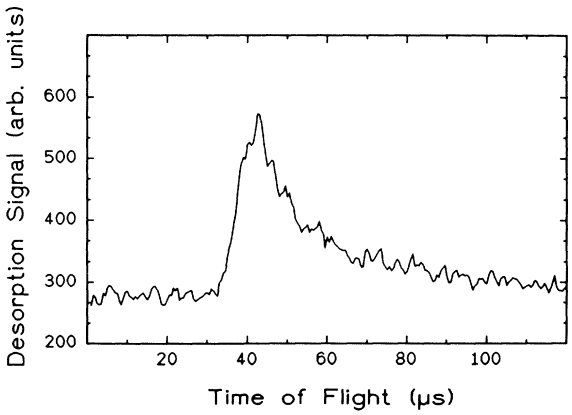

FIG. 10. Time-of-flight spectrum of Na atoms desorbed with laser light of 514 nm from the surface of small Na particles. The measured flight times have to be corrected for the drift time of the ions in the quadrupole mass spectrometer (18 μs).

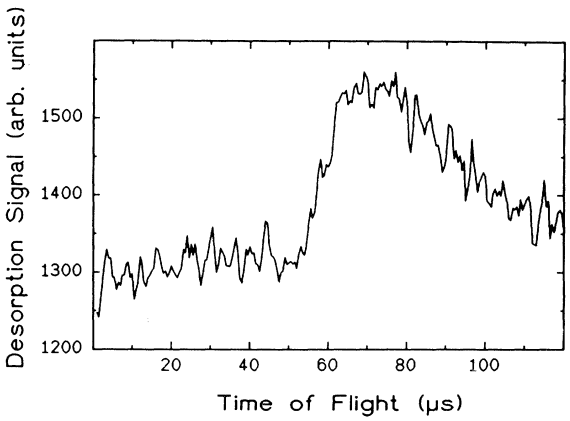

FIG. 11. Time-of-flight spectrum of K atoms desorbed with laser light of 514 nm from the surface of small K particles. The measured flight times have to be corrected for the drift time of the ions in the quadrupole mass spectrometer (22 μs).

steep rise, followed by a maximum and a slow decrease of the rate as a function of time. For sodium, e.g., the Na signal starts to increase 33 ± 2 μs after firing the light pulse, and a sharp maximum occurs at 42 ± 2 μs. Even after as much as 120 μs the signal has not yet decayed to the noise level recorded prior to the laser pulse. It seems that this slow decrease does not reflect desorption with low kinetic energies but is due to atoms which do not reach the ionization region directly, but only after suffering collisions, with, e.g., the electrodes of the ionizer. For all spectra the energy of the desorbed atoms was derived from the position of the maximum of the time-of-flight distribution. It should be mentioned that these spectra cannot be fitted to Maxwellian distributions.

Measurements have also been carried out with different excitation wavelengths. The dependence of the flight time of the desorbed atoms on the laser wavelength is displayed in Fig. 12 for Na. Small but significant variations are observed. For wavelengths close to the maximum of the desorption rate at $\lambda=490$ nm (see Fig. 3), i.e., at a photon energy of $E_{ph}=2.53$ eV, the flight time is 24 μs (see Fig. 12). This corresponds to a kinetic energy of 0.4 ± 0.05 eV.[26] For larger as well as smaller wavelengths, the kinetic energy decreases. For example, a value of 0.2 eV is obtained for $E_{ph}=3.54$ eV ($\lambda=350$ nm). For potassium no change of the flight time as a function of photon energy was observed. The kinetic energy of the desorbed K atoms is 0.13 ± 0.02 eV. Measurements have also been performed for different laser intensities and different particle temperatures. A remarkable observation is that the flight time is independent of temperature and laser pulse energy in the investigated ranges of $90 < T < 300$ K and 5 μJ to 10 mJ, respectively. If the laser pulse energy is increased to values above 10 mJ, the flight time of the atoms decreases, probably because thermal desorption also comes into play. Adsorption of molecules on the surface of the metal particles does not cause a detectable change of the time-of-flight spectra.

The same set of measurements was made for potassium. The observed dependencies on the laser power and

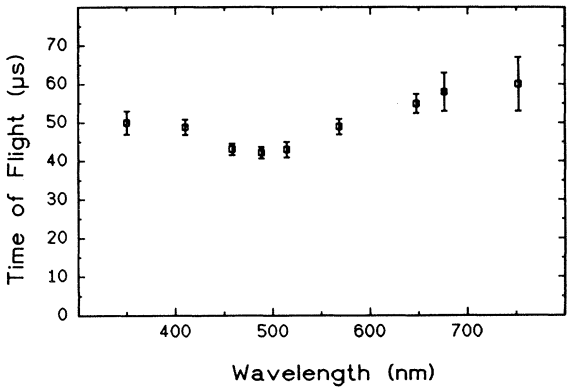

FIG. 12. Dependence of the time of flight of the desorbed Na atoms on the laser excitation wavelength measured for an average particle radius of 38 nm. The plotted values *include* the drift time of the Na ions in the mass spectrometer (18 μs). The measured values correspond to the following kinetic energies of the desorbed atoms: 40 μs, 0.45 eV; 42.5 μs, 0.36 eV; 45 μs, 0.29 eV; 50 μs, 0.20 eV; and 60 μs, 0.11 eV.

particle temperature are very similar to those of sodium. For the reasons given above, time-of-flight measurements on Ag atoms will have to be performed in future experiments.

D. Measurement of optical spectra

Optical spectra have been recorded for two purposes: first, such investigations are helpful in order to identify the optical excitation preceding the rupture of the bond of a metal atom. Second, the optical spectra constitute an important tool to characterize the average size and shape of the metal particles generated on the LiF surface. For these reasons the transmission spectra of Na, K, and Ag particles were measured for wavelengths between 250 and 950 nm. The substrate temperature was $T \approx 100$ K. Examples are displayed in Fig. 13. For sodium [see Fig. 13(a)] the mean particle radii ranged from 41 to 92 nm. A broad maximum is observed that shifts from $\lambda \sim 600$ to $\lambda \sim 750$ nm if the particles increase in size. The optical extinction grows to as much as 65%. For wavelengths below 400 nm, small but reproducible peaks also appear in the spectra of the clusters with $R = 73$ and 92 nm. Figure 13(b) shows examples of the optical spectra of potassium particles with mean particle radii that varied from 60 to 140 nm. The spectra have in common that an overall increase of the extinction with increasing wavelength takes place. For wavelengths between $\lambda = 400$ and 550 nm a plateau is observed initially. For larger particle radii two distinct maxima located at $\lambda = 425$ and 495 nm appear. The peak positions of these maxima do not shift as a function of radius. Finally, Fig. 13(c) displays spectra of Ag particles with mean radii between 16 and 40 nm. The most prominent feature of the Ag spectra is a broad maximum that shifts from $\lambda = 375$ to 510 nm. Simultaneously, the extinction increases from 9% to as much as 77%. At $\lambda = 365$ nm a shoulder appears which does not shift as a function of coverage. Below $\lambda = 325$ nm the extinction increases as a function of particle size due to interband transitions.

It is well known and will be discussed below that the broad maxima observed in all of the spectra of the metal particles are due to surface plasmons, i.e., collective dipole excitations of the conduction electrons at the cluster surface.[27] The origin of the additional signals with narrower widths and smaller amplitudes is not completely clear. They could result, for example, from excitation of quadrupole modes.

III. DESORPTION MECHANISM

The results summarized above permit us to draw several conclusions.[2–5]

(i) First, desorption obviously results from electronic excitation of the particles. Comparison of the dependence of the desorption rate on the laser wavelength with

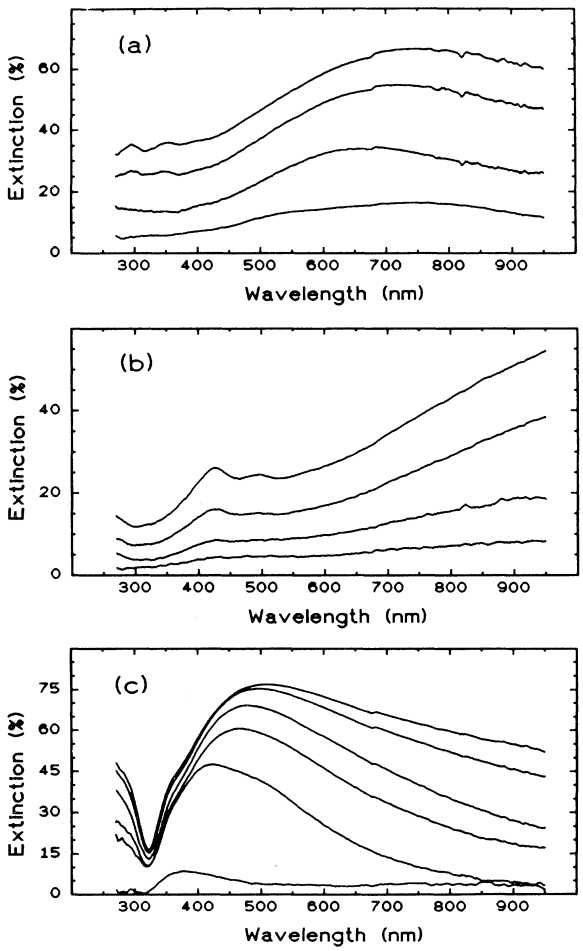

FIG. 13. Optical extinction spectra of different metal particles supported on LiF(100). The measurement were made with a Xe arc lamp and a monochromator under normal incidence of the light on the LiF substrate. (a) Spectra of Na particles at $T = 100$ K for average radii of 41, 58, 73, and 92 nm. (b) Spectra of K particles at $T = 100$ K for average radii of 60, 80, 91, and 140 nm. (c) Spectra of Ag particles at $T = 250$ K for average radii of 16, 31, 34, 36, 38, and 40 nm.

the optical spectra of the particles indicates that surface plasmon excitation plays a decisive role in stimulating desorption.[4]

(ii) Second, rupture of the surface chemical bond of the metal atoms takes place as a nonthermal effect, i.e., the electronic excitation energy is not or is not completely quenched by conversion into heat before the atoms escape from the surface potential. This conclusion is supported by the high kinetic energy of the desorbed atoms, by its independence on the laser power, and by the fast response of the desorption rate if the light beam is blocked or unblocked. Also, there is no threshold of the desorption rate at low laser power. Estimates of the temperature rise at the particle surface, and measurements with adsorbate molecules (see above) further indicate that the temperature increases by at most several tens of degrees under irradiation with laser powers of several W.

(iii) Third, the linear dependence of the desorption rate on the laser power indicates that a single photon process is responsible for the detachment of a metal atom.

These conclusions give an overall description of the process. However, they do not explain details of the desorption mechanism. In particular, it is not conceivable why desorption should occur as a result of surface plasmon excitation alone. Such a collective oscillation of the conduction electrons extends over the whole surface of the metal particles, whereas the detachment of atoms must take place from well-defined binding sites. Therefore, a localized single-electron excitation must also be involved which obviously *communicates* with the collective mode. Identification of this localized electronic excitation is an important step toward an understanding of the mechanism of metal-atom desorption. Its nature as well as its interplay with the collective excitation will be discussed in the following sections.

A. Electronic excitation and classical electrodynamics

It is well known that the classical Mie theory[28] describes the optical spectra of small spherical particles very well in the size range considered here.[29–31] Therefore, the first step of the interpretation naturally is to compare the dependence of the desorption rate on the cluster radius and on the excitation wavelength with theoretical absorption spectra calculated using the Mie theory. Since the theoretical framework of the Mie theory and the calculation of the spectra have been described in detail elsewhere,[4] only a short summary will be given here.

Within the framework of the Mie theory the interaction of spherical particles with light is treated by a multipole expansion of the electromagnetic field and by solving Maxwell's equations with appropriate boundary conditions. Input parameters are the bulk optical function $\epsilon(\omega)$ of the particles, and the index of refraction of the surrounding medium. Since the particles investigated here have radii on the order of 5–100 nm, i.e., the size is not small as compared to the excitation wavelength of the incident light, higher-order multipole resonances and phase retardation must be considered. Taking these effects into account, the cross sections for extinction σ_{ext}, scattering σ_{sca}, and absorption σ_{abs} were calculated as a function of radius and wavelength. For this purpose a computer program based on an earlier version of Bohren and Huffman[32] was developed. The computation was done first for particles of a single size, and then extended to cluster size distributions known from electron microscopy work (e.g., Refs. 31, 33, and 34). As an approximation for the influence of the substrate, it was assumed that the particles can be considered as embedded in a matrix with an average index of refraction of $n_{av}=1.15$. This value is chosen such that it lies in between the vacuum value and the value of the LiF substrate of $n_{LiF}=1.39$. Optical functions were taken from Ref. 35 for sodium, and from Ref. 36 for potassium. Calculation of the *extinction* cross sections allows comparison with the experimental spectra as displayed in Fig. 13, and permits us to estimate the mean particle size and shape.[22] Computation of the *absorption* spectra, on the other hand, suggests itself to explain the radial and spectral dependence of the desorption rate.

Figure 14 shows the absorption cross section of Na particles as a function of the wavelength and mean cluster radius. The width of the distribution is 50% of the mean cluster radius. For large particle radii the cross sections increase rapidly. This behavior results from excitation of quadrupole as well as modes of even higher multipole order. In general, the absorption cross sections of the Mie theory follow the measured desorption data quite well. Therefore, it has been concluded earlier that surface plasmons play an important role for stimulating desorption. However, a detailed comparison between theory and experiment on the basis of the data available now reveals deviations. The most remarkable difference between the theoretical curves and the measured data is observed for large cluster radii. Whereas the computed absorption cross sections continue to grow for increasing radii, the experimental desorption rates (see Fig. 4) go through a maximum and then continuously drop off. This has been verified for radii as large as 150 nm. Also, differences between theory and experiment appear for short excitation wavelength independent of cluster size (see Fig. 3). Whereas the absorption cross sections con-

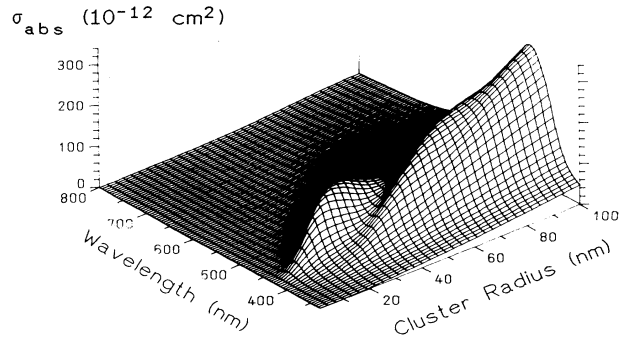

FIG. 14. Optical-absorption spectra of Na particles computed with the Mie theory as a function of wavelength and particle size. The influence of the substrate is taken into account by treating the particle as embedded in a medium with an average index of refraction of 1.15.

tinuously decrease for short wavelengths, the desorption rates exhibit a minimum at approximately $\lambda=410$ nm, and increase again below $\lambda<400$ nm.

B. Electron spill-out and nonlocal optical effects

As outlined above, the interaction of light with metal spheres is theoretically well described by the Mie theory. Basic assumptions of this theory are the spatial uniformity of the complex dielectric function $\epsilon(\omega)$, its local character, and its steplike change at the particle surface. For isotropic materials the classical dielectric displacement $\mathbf{D}^{\mathrm{cl}}$ in the interior of the particle is described by the local equation with scalar $\epsilon(\omega)$ of the bulk:

$$\mathbf{D}^{\mathrm{cl}}(\omega,\mathbf{r},t)=\epsilon(\omega)\mathbf{E}^{\mathrm{cl}}(\omega,\mathbf{r},t)\ . \tag{1}$$

The word "local" in this context means that the response of the medium to an incident electromagnetic wave at the point $\mathbf{r}$ is independent of the dielectric surrounding. For the steplike change of the electron charge density at the cluster surface, an electromagnetic wave gives rise to a singularity in the induced surface charge and a discontinuity in the radial electric field.[37]

Certainly, the assumption of a sharp edge of the electron charge density at the particle surface is not justified on a microscopic scale. In a more elaborate model a gradual change of the electron density including a spill-out has to be considered. Nevertheless, numerous experiments have verified the results computed by the Mie theory.[31] The reason is that the incident light penetrates many Å into the interior of the particles. In other words, absorption and scattering of light depend mainly on the bulk properties of the particle making physical details of the surface region unimportant. Furthermore, a variety of other effects, such as deviation from spherical shape, interaction of the particle with the substrate, or size dependences of the optical functions, can considerably modify the optical spectra. In short, the optical spectra of small particles usually do not contain information on details of the electron-density distribution in the surface region. Such details, however, become essential if surface specific processes are investigated. Examples are the emission of electrons[38,39] or the case considered here, i.e., desorption of surface atoms. To stimulate these reactions, electronic excitation in the surface layer rather than in the bulk of the cluster must be accomplished. The required additional absorption of light in the surface region, not contained in the framework of the Mie theory, can only be understood and separated from the bulk excitation by use of a microscopic model of the surface. It takes into account the spill-out of the electron charge mentioned above and, in addition, nonlocal optical effects. Both will be discussed in the following.

Metal surfaces are often described by the *jellium* model. It assumes that the true, spatially periodic charge distribution of the ion cores can be replaced by a homogeneous density that has a sharp edge at the surface. The electron-density distribution is calculated self-consistently, and shows a spill-out beyond the edge of the ion cores. This spill-out is found for planar surfaces[40] as well as for the surface of spherical particles.[41] The surface charge which is induced by an external electromagnetic field also exhibits a pronounced radial dependence, i.e., the electron spill-out removes the singularity mentioned above. Also, the discontinuity of the radial electric field disappears. The length over which the surface charge relaxes is influenced by the distance an electron travels during one oscillation period of the external field, i.e., by the Fermi wavelength being of the order of several Å.[37]

Furthermore, a microscopic theory with the goal of describing the response of a metal cluster to an incident electromagnetic wave must take *nonlocality* into account. Nonlocal means that the dielectric displacement $\mathbf{D}(\omega)$ of a volume element $dV(\mathbf{r})$ at time t does not depend only on the electric field $\mathbf{E}(\omega,\mathbf{r},t)$ of the incident wave, but also on the excitations and fields in all other volume elements $dV(\mathbf{r}')$ of the cluster occurring at properly retarded times t'. The polarizability $\alpha(\mathbf{r})$ of $dV(\mathbf{r})$ can be influenced by the polarization at the point $\mathbf{r}'$ that is induced by the same field. For example, electrons excited in $dV(\mathbf{r})$ can transfer their energy and momentum to other volume elements $dV(\mathbf{r}')$ located within the electron mean free path. For metals the value is on the order of 10 nm. Nonlocal effects play a particularly pronounced role in the surface region of a metal where the electric field varies considerably between the bulk and vacuum values over a distance of only a few Å. Since the generation of large field variation is associated with losses, this transition region provides new channels for the dissipation of energy in addition to the usual Joule heating: the incident light induces electron-hole pairs in the surface region.

Before the surface absorption that is responsible for stimulating desorption of atoms can be calculated, we first have to replace the local equation (1) by its nonlocal equivalent[38]

$$\mathbf{D}(\omega,\mathbf{r},t)=\int dt'\int d^3r'\{\epsilon(\omega,\mathbf{r},\mathbf{r}',t-t')\mathbf{E}(\omega,\mathbf{r}',t')\}\ , \tag{2}$$

where $\epsilon(\omega,\mathbf{r},\mathbf{r}',t-t')$ is the nonlocal dielectric function. Unfortunately, it is not known in detail for the surface of real metals. Another complication is that the mathematical formalism for solving Eq. (2) is very complicated. For both reasons, only approximate solutions of Eq. (2) are described in the literature.[19,37,42–45]

The dielectric displacement $\mathbf{D}$ can be used to express the *total* normalized power of an electromagnetic wave that is absorbed by a small metal sphere:[45]

$$a(R,\omega)=-\frac{\omega}{8\pi I_0}\mathrm{Im}\left\{\int d^3r\,\mathbf{D}^*\cdot\mathbf{E}\right\}\ . \tag{3}$$

The difference between the absorption calculated with nonlocal optics by Eq. (2), and its classical local counterpart, then gives the surface contribution a_{sur} of the absorbed power. Strictly speaking this is valid only if the absorption in the surface layer is small as compared to the bulk.[45] This condition is fulfilled in the present work, the investigated clusters having sufficiently large radii. Since the most pronounced difference of the classical and nonlocal pictures is the variation of the radial electric field in the surface region, a_{sur} can be calculated to a

reasonable first approximation from

$$a_{\rm sur}(R,\omega)=-\frac{\omega}{8\pi I_0}\,{\rm Im}\left\{\int d^3r\, D_r^*(E_r-E_r^{\rm cl})\right\}, \quad (4)$$

where $E_r^{\rm cl}$ and E_r are the electric field at the surface for the classical local and nonlocal cases, respectively. Equation (4) can be solved within the quasistatic approximation, i.e., for spheres which are small compared to the wavelength of the incident light.[46] One obtains (see, e.g., Refs. 19, 38, 42, and 45)

$$a_{\rm sur}(R,\omega)=\frac{4}{3}\frac{\omega}{c}R\left|\frac{\epsilon E_r^{\rm cl}(R,\omega)}{E_0}\right|^2 {\rm Im}\left[\frac{1-\epsilon}{\epsilon}\frac{d_r}{R}\right], \quad (5)$$

where E_0 is the amplitude of the incident light wave, and d_r denotes the complex surface response function, defined by

$$\frac{d_r(\omega)}{R}=\frac{\int dr\, r(R-r)\delta\tilde{\rho}_r}{\int dr\, r^2\delta\tilde{\rho}_r}. \quad (6)$$

In Eq. (5) the surface part of the absorption depends only on (i) the complex surface response function $d_r(\omega)$ which accounts for all nonlocal effects; (ii) the *local* dielectric function $\epsilon(\omega)$ that is well known for bulk metals; and (iii) the normalized classical electric field $E_r^{\rm cl}$ at the particle surface which can be calculated from the Mie theory. The quantity $\delta\tilde{\rho}_r$ in Eq. (6) is related to the induced surface charge density $\delta\rho(R,\omega)$ by $\delta\rho(R,\omega)=\delta\tilde{\rho}_r\cos\theta$; θ is the angle between the direction of the incident light and the normal of the surface element. Since d_r is related to the induced surface charge $\rho(R,\omega)$ its physical meaning can be understood as follows. The real part of d_r is interpreted as the distance of the center of gravity of the induced surface charge from the edge of the positive ion core. The imaginary part of d_r, on the other hand, describes the surface absorption. It results from the single-electron excitations mentioned above and often denoted as electron-hole pair formation in the surface region (see, e.g., Refs. 38 and 45). d_r has been calculated as a function of excitation frequency for a free-electron gas,[47] a case which resembles the situation at the surface of alkali metals.

C. Desorption rate and surface absorption

After this explanation of the physical origin of the surface absorption, we now turn to a quantitative description of the desorption rate dN/dt as a function of excitation frequency and particle size. For this purpose it is plausible to assume that the desorption rate is related to the absorption $a_{\rm sur}(R,\omega)$ within the surface layer, i.e., that electron-hole pair formation in the surface region is responsible for the rupture of the bond of surface atoms. Furthermore, the desorption rate should depend on the incident photon flux $I_0/\hbar\omega$, on the cluster density $\rho_{\rm clu}$, and on the irradiated surface area F. This gives[19]

$$\left.\frac{dN}{dt}\right|_{t=0}=A_{\rm eff}(R)a_{\rm sur}(R,\omega)\frac{I_0}{\hbar\omega}\rho_{\rm clu}F. \quad (7)$$

The subscript $t=0$ of the desorption rate indicates that Eq. (7) is valid only for a short interval of time immediately after directing the laser beam onto the freshly prepared clusters. The temporal dependence of the desorption rate for $t\geq 0$ is determined by the variation of cluster size and shape during continuous detachment of atoms, and has been discussed elsewhere in a phenomenological model.[24]

1. *Efficiency factor* $A_{\rm eff}$

According to a concept introduced by Monreal and Apell,[19] $A_{\rm eff}$ is an efficiency factor which has the dimension of a surface. It accounts for two effects.

(i) The number of desorption sites. The surface of each cluster contains only a certain number of sites from which atoms are able to desorb. It has been shown experimentally that *thermal* desorption preferentially takes place from sites with a low coordination number.[21] These sites can, for example, be located on top of monocrystalline terraces or on edges of the cluster surface where planes with different crystallographic orientation intersect. Each of these sites can be regarded as an element that represents surface roughness, i.e., a defectlike structure, where localized electronic excitation can easily be accomplished. Similar to thermal desorption it is assumed here that nonthermal detachment of metal atoms primarily takes place from sites with a low coordination number and therefore low cohesive energy.

(ii) The quantum efficiency of the desorption process. Coupling of the electronic excitation to vibrational modes, i.e., generation of heat, constitutes a relaxation channel that competes with desorption. Therefore, absorption of a certain number of photons is necessary in order to desorb one surface atom. Since the metal particles considered here are relatively large in size, bulklike electron-phonon coupling can be assumed. Consequently, the quantum efficiency of the desorption is regarded as independent of cluster size. As mentioned above it is on the order of 10^{-4} for excitation by frequencies within the surface plasmon resonance.

The dependence of $A_{\rm eff}$ on the cluster radius can be inferred from the following consideration. For very small particles almost all of the atoms contribute to surface roughness, i.e., constitute defects. If they increase in size, the ability to desorb is confined to the surface atoms. The ratio of the number of surface atoms to the total number of atoms $N_{\rm surf}/N_{\rm tot}$ decreases only slowly from unity with increasing size. One can assume as a first approximation that the number of desorption sites is proportional to R^3 for very small clusters, and to R^2 for medium-size particles. This is indeed observed experimentally (see Fig. 5). Up to $R=5$ nm the desorption rate grows with R^3, whereas for $R\geq 5$ nm a quadratic dependence is observed.[48] If the particles grow even larger, the different crystalline facets of the surface are more extended, making desorption possible only from a limited number of surface sites such as kinks or steps on the cluster surface. A reasonable assumption therefore is that the number of desorption sites is proportional to R for large clusters. This is supported by thermal desorption experiments[21] which indicate a linear dependence of the num-

ber of desorption sites on the particle radius for $R \geq 20$ nm. In summary, A_{eff} exhibits only a weak, monotonous dependence on the cluster radius in the size range considered here.

2. *Surface absorption* $a_{\text{sur}}(R,\omega)$

Since the imaginary part of the surface response function $\text{Im}\{d_r\}$ is almost independent of particle size,[19] the radial and spectral dependence of $a_{\text{sur}}(R,\omega)$ is dominated by the frequency and radius dependence of the field enhancement $E_r(R,w)/E_0$. It can be computed with the Mie theory. The field enhancement is analytically given by[49]

$$\frac{E_R^2}{E_0^2} = \frac{2\pi}{k^2} \sum_{j=1}^{\infty} (2j+1)(j+1)j|a_j|^2|h_j^{(2)}(kR)|^2 , \quad (8)$$

where a_j denotes the electric scattering coefficient, j the multipole order, and $h_j^{(2)}$ the second-order Hankel function. The near field has been calculated as a function of R and ω. For this purpose the same parameters as in Fig. 14 were used, i.e., the average index of refraction was $n_{\text{av}}=1.15$, and the width of the cluster size distribution was 50% of the mean particle size. The result of the computation is displayed in Fig. 15 as a function of particle radius and excitation wavelength. The diagram exhibits a single maximum that originates from excitation of the electric dipole oscillation. It is located at $\lambda=420$ nm and $R=6$ nm. The ratio $[E_r(R,w)/E_0]^2$ can amount to as much as 1000. The values for the field enhancement obtained here are within the range reported in several other papers in the literature. Note that Ref. 19 quotes values of around 3, which, however, do not contradict our results based on Ref. 49, since the two theories define the field enhancement in different ways. Comparison of Fig. 15 with the optical-absorption spectra shows pronounced differences. The most essential one is that higher-order multipoles contribute only little to the field enhancement. Particularly for large clusters this is in sharp contrast to the optical absorption spectra (Fig. 14), the shape of which is strongly influenced by excitation of multipole oscillations with $n \geq 2$. The difference between the near field at the surface and the far field can be understood as a tip effect that arises at the particle surface with its small radius of curvature. In accordance with Fig. 15 this effect is expected to disappear for large clusters. In summary, excitation of surface plasmons dramatically enhances the near field at the surface of the metal particles in the size range up to approximately $R=50$ nm.

D. Comparison to experiment

As discussed above, the desorption rate dN/dt depends on the efficiency factor A_{eff} as well as on the absorption of light $a_{\text{sur}}(R,\omega)$ in the surface region of the metal particles. A_{eff} varies only weakly and monotonously with cluster size for $R \geq 20$ nm. The dependence of the surface absorption $a_{\text{sur}}(R,\omega)$, on the other hand, is governed by the radial and spectral dependence of the near-field enhancement that changes resonantly by about a factor of 1000 in the size and wavelength ranges investigated here. Therefore, the experimental results have to be compared primarily to the variation of the field enhancement. This can best be done by using the data of the overview Fig. 15 to plot the enhancement factor $E_r(R,\omega)/E_0$ as a function of wavelength with typical cluster radii as parameters and vice versa. Such diagrams are depicted for sodium clusters in Figs. 16 and 17 for typical radii and wavelength used experimentally. Clearly, the field enhancement exhibits a resonance if the particle radius is kept constant and the wavelength changes, or vice versa. The highest values of the field enhancement occur for the Kr^+-ion laser lines around $\lambda=410$ nm, and the Ar^+-ion laser line at $\lambda=458$ nm. For longer excitation wavelengths, the maximum of the dipole oscillation is shifted to larger cluster radii. Due to the tip effect, small clusters show the most pronounced maximum. It is located at a wavelength of about $\lambda=450$ nm, and shifts only little

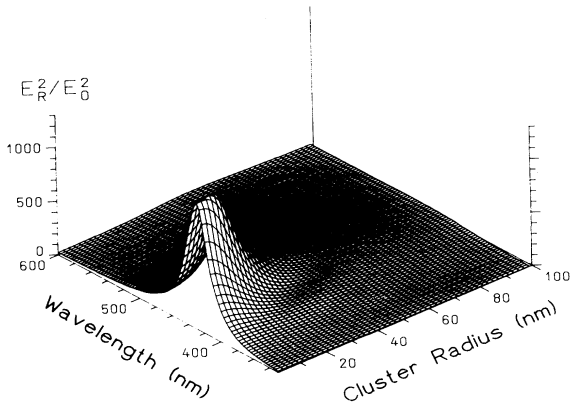

FIG. 15. Enhancement of the radial electric near field at the surface of Na particles as a function of particle radius and wavelength of the incoming light. The width of the particle size distribution was 50% of the average size. The influence of the substrate was taken into account by treating the particle as embedded in a medium with an average index of refraction of 1.15.

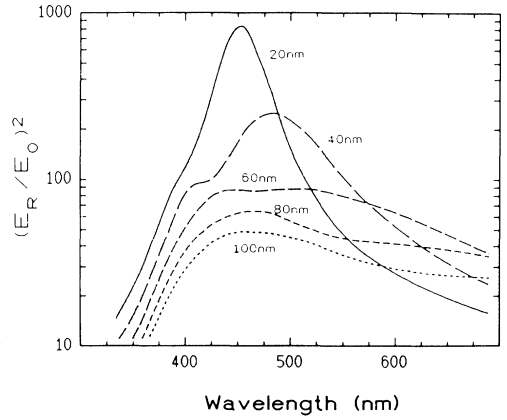

FIG. 16. Enhancement of the radial electric near field at the surface of Na particles as a function of wavelength for several fixed particle radii. Conditions are the same as in Fig. 15. A detailed comparison of the theoretical data shown here with the experimental results contained in Fig. 3 can be found in Sec. III D.

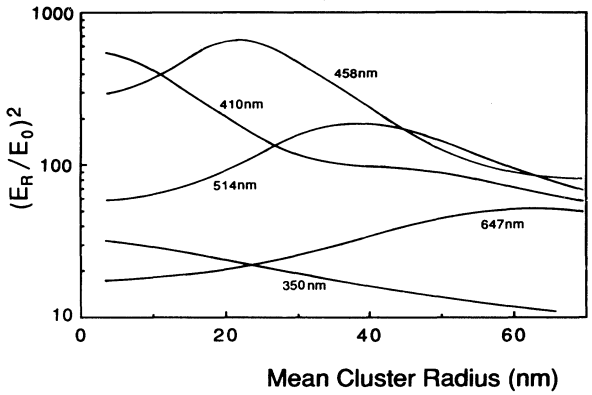

FIG. 17. Enhancement of the radial electric near field at the surface of Na particles as a function of particle radius for several fixed laser wavelengths. Conditions are the same as in Fig. 15. Section III D of the text gives a detailed comparison with the experimental results that are contained in Fig. 4.

if the particles increase in size.

Comparison of the experimental data (see Fig. 4) with the theoretical results of the near-field enhancement as a function of mean cluster radius (see Fig. 17) leads to the following conclusions. For laser wavelengths of $\lambda=458$, 514, and 647 nm the experimental data follows the trend of the field enhancement as a function of radius. As predicted by the theoretical data, the positions of the maxima of the resonance curves shift to larger particle radii if the excitation wavelength increases. Furthermore, the desorption rate decreases monotonously for large cluster radii (see the right-hand side of Fig. 4), a trend that could be verified for particles as large as 150 nm (see above). Again, this observation is in good agreement with the variation of the near-field enhancement. As outlined above, however, it is in contrast to the optical absorption, the cross section of which grows further and further for large radii (see Fig. 14).

For excitations wavelengths of $\lambda=350$ and 410 nm the experimental data do not follow the computed field enhancement. $[E_r(R,\omega)/E_0]^2$ grows monotonously if the clusters shrink in size (see Fig. 17), whereas the desorption rate exhibits a pronounced maximum. In general, the desorption rates for particles with $R \leq 20$ nm tend to be smaller than expected from the dependence of the field enhancement. This is also visible in the curves for $\lambda=458$, 514, and 647 nm (see Fig. 4). The influence of this effect becomes more and more pronounced as the wavelength decreases, and the resonance shifts to shorter wavelength. The reason is that the dependence of the desorption rate is not determined by the field enhancement alone in this size range. For particles with $R \leq 20$ nm, the efficiency factor A_{eff} increasingly influences the change of the desorption rate (see above). Since A_{eff} is proportional to R^2 rather than to R in this size regime, the number of available desorption sites decreases rapidly with shrinking radius. Therefore, the influence of A_{eff} becomes more and more pronounced. As a consequence, the product of $[E_r(R,\omega)/E_0]^2$ and A_{eff} [see Eqs. (8) and (7)] can exhibit a resonancelike dependence on the particle size exactly as observed experimentally (see Fig. 4). This effect depends on the position of the resonance: if it is located at radii larger than $R \cong 20$ nm, the desorption rate is already low for small radii and the size dependence of the efficiency factor does not significantly change the shape of the curve. However, if the desorption rate is large for $R \leq 20$ nm, the strong decrease of A_{eff} with cluster size overcompensates for the slow increase of the field enhancement, so that a resonance for excitation with $\lambda=350$ and 410 nm appears. The influence of A_{eff} also manifests itself by the very small shift of the resonance radius measured at wavelengths below $\lambda=458$ nm. Regardless of the field enhancement, the size dependence of A_{eff} for small clusters causes an almost fixed resonance position.

Another test of the theoretical approach outlined above is to compare the wavelength dependencies of the desorption rate and field enhancement. As can be seen from Figs. 3 and 16, experiment and theory agree quite well for wavelengths above $\lambda=400$ nm. Resonances located between $\lambda=450$ and 500 nm appear in both cases. They shift only little with cluster size. The predicted decreasing *maximum* desorption rate with increasing particle size above 22 nm (see Fig. 16) is also well reproduced experimentally. The curve of the field enhancement for $R=20$ nm exhibits a larger maximum value as compared to the dependence of the desorption rate on the laser wavelength ($R \approx 22$ nm). Again, this is indicative of the rapidly decreasing value of A_{eff} in this size range, i.e., the available number of desorption sites (see above). This effect plays an even larger role if the particle radius decreases further to a value of $R=12$ nm (see Fig. 3). For excitation with UV light at $\lambda=350$ nm, the desorption rates are larger than expected from the wavelength dependence of the field enhancement. The most probable reason is that the imaginary part of the surface response function $\text{Im}\{d_r\}$ [see Eq. (6)] increases at short wavelengths[47] by such an extent that the decrease of $[E_r(R,\omega)/E_0]^2$ is overcompensated for.

The result for potassium can be analyzed in a similar manner. For this purpose the field enhancement was also calculated as a function of cluster radius and excitation wavelength. The same size distribution as for Na, and the same average index of refraction n_{av} was used in the computation. The maximum enhancement occurs at $\lambda=605$ nm and $R \approx 5$ nm. The main differences as compared to Na are, on the one hand, a shift of the maximum field enhancement for a given laser wavelength toward smaller particle radii. On the other hand, the dependence of the enhancement on the cluster radius is much less pronounced for radii below 30 nm. Therefore, the size dependence of the efficiency factor A_{eff} as discussed above has a much more pronounced influence on the spectra for $R < 50$ nm. In particular, the desorption rate decreases rapidly between about 30 and 50 nm independent of excitation wavelength (see Fig. 6). This steep decrease reflects the change of the efficiency factor rather than the small variation of the enhancement factor with size. Whereas A_{eff} began to play an essential role for $R \leq 20$ nm in the case of Na, it has a strong influence on the K desorption rate for $R \leq 50$ nm. This can be under-

stood by the larger nearest-neighbor distance of 5.2 Å in potassium as compared to 4.2 Å in sodium, so that A_{eff} starts to decrease rapidly at a larger particle radius. Similar to Na the dependence of the desorption rate on the wavelength for a fixed cluster radius follows the trend of the calculated field enhancement. The only exception is an increase of the desorption rate for short wavelengths that was also found for Na. Again, this is attributed to an increase of the imaginary part of the surface response function $\mathrm{Im}\{d_r\}$.

In summary, the agreement of the experimental results with the dependencies expected from Eq. (7) confirms the propounded model based on nonlocal optical effects and on a realistic electron-density distribution in the surface region of the clusters. Particularly pronounced is the influence of surface plasmon excitation on the size and wavelength dependence of the desorption rate. It causes a strong enhancement of the near field at the surface by which excitation of electron-hole pairs becomes possible. These single-electron excitations obviously are responsible for stimulating desorption of surface atoms. The underlying mechanism will be discussed in more detail in Sec. III E.

E. Desorption mechanism and discussion

As explained above, nonlocal optics provides the first step to an understanding of the desorption process, i.e., the transformation of photon energy into electron excitation. In a subsequent step, relaxation of the electronic excitation occurs through two channels. First, coupling to the phonon bath of the particle, i.e., generation of heat, takes place. The small quantum efficiency of the desorption process of 10^{-4} indicates that this constitutes the dominant process. Second, desorption of surface atoms occurs. This requires population of an antibonding state. It is energetically different from the one excited initially. This can be seen from the energy balance of the process: The absorbed photon energy E_p ranges from 2 to 3.5 eV; the binding energy E_b of a surface atom, on the other hand, is 0.7 eV for Na,[20] and 0.6 eV for K, and the measured kinetic energy E_k of the detached atoms amounts to several tenths of an eV. Therefore, the sum of E_k and E_b is considerably smaller than E_p. Consequently, desorption must take place from an antibonding state into which the original electron-hole pair decays by conversion of part of the electronic energy into heat. The energy balance shows that this state is located approximately 1.1 eV above the ground state. This energy value lies within the gap above the conduction band, and can therefore be described by a localized wave function.

A remarkable observation is that the kinetic energy of the desorbed atoms depends on the excitation wavelength (see Fig. 12). This is quite surprising since the electron-hole pair populated initially decays into a second state in the course of which part of the energy is converted into phonons. It seems that this repulsive level from which desorption finally takes place has retained a memory of the original excitation. The reason for this is presently not understood. A wavelength-dependent kinetic energy in the vicinity of the surface plasmon resonance has also been observed in experiments on laser-stimulated desorption of metal ions.[50]

When the particles are irradiated with light, absorption is possible through two channels. First, collective Mie resonances that decay by generation of heat are excited. Second, nonlocal optical effects cause additional absorption of light in the surface region of the clusters by single-electron excitation. The electron-hole pairs created relax into antibonding levels. As a consequence, an atom can gain sufficient kinetic energy to escape from the surface potential so that desorption eventually occurs. At different stages during the process, electron-phonon coupling takes place and heat is released.

The number of generated electron-hole pairs is proportional to the value of the radial electric near-field intensity at the surface, which in turn is enhanced by excitation of the collective mode. One could say that the surface plasmon acts as a catalyst that promotes excitation in the surface region of the particles and makes desorption detectable. The energy-level diagram of the desorption reaction is displayed in Fig. 18. The metal atom that eventually desorbs is treated as an adsorbate on a flat metal surface. Rupture of the bond can take place along the lines of the well-known Menzel-Gomer-Readhead scenario from antibonding states designated as $(M+A)^*$. M stands for the surface of the metal cluster, and A for an atom on this surface. Desorption is assumed to occur from a defect, i.e., from a site where the metal atoms are not arranged in plane terraces. More generally speaking, such a structure can be associated with surface roughness. In Sec. III C this concept already has been used to estimate the efficiency factor A_{eff} as a function of the particle radius. Here it is helpful to discuss the nature of the electron-hole pair excitation and the repulsive state. As mentioned earlier, the coordination number of an atom on a flat surface is particularly low, causing a small binding energy. In addition, the conduction electrons in the vicinity of a defect are not completely delocalized as in

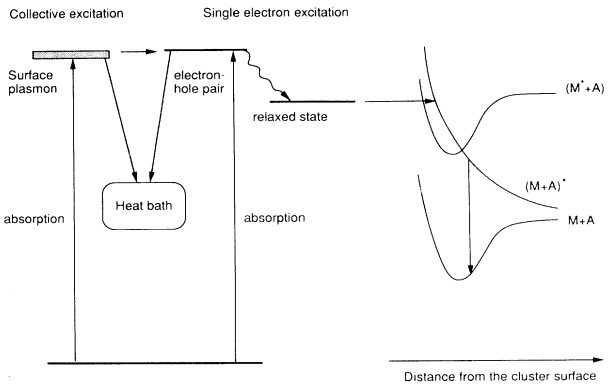

FIG. 18. Schematic diagram of the desorption process. Left-hand part: Photon absorption causes generation of electron-hole pairs in the surface layer of the particle. The excitation rate is catalytically enhanced by simultaneous excitation of surface plasmons. Right-hand part: Aside from coupling to the heat bath, transitions to antibonding states $(M+A)^*$ result in atom desorption.

the bulk. The wave functions of ground and excited states are correlated to resonances within the band gap of the metal. As a result of the partial localization, coupling to the phonon bath is reduced, although still prevalent, and a metal atom can escape from the surface potential with a finite probability.

Is there, however, experimental evidence for preferential desorption from defects? Direct proof can provide the deliberate change of the number of such sites and the measurement of the resulting variation of the desorption rate. If the particle temperature is raised, for example, the number of surface defects should increase since atoms can be detached more likely from steps, edges, and kinks, or even lifted out of the terraces. The number of the created defects and therefore the desorption rate is expected to increase as $\exp[-(E_A/kT)]$, T being the temperature, and E_A the activation energy for generation of structural defects. Indeed, Fig. 8 shows that the desorption rate for Na varies exactly in the manner predicted as a function of temperature. The activation energy is $E_A = 0.14$ eV.

This model of the desorption process also suggests itself quite naturally as an explanation for the detachment of metal atoms from thin metallic films. Such films usually exhibit a certain roughness, i.e., a large number of structural defects in the sense described above. Indeed, nonthermal desorption of Au, Ag, and Al atoms has been observed from thin films in which surface plasmons were excited with pulsed laser light in an attenuated total reflection (ATR) geometry.[8] The measured kinetic energies are 0.9, 0.33, and 0.51 eV for Ag, Au, and Al atoms, respectively. Whether or not desorption of metal *ions* with kinetic energies as high as several eV (Refs. 10 and 51) can also be explained along the lines of the model discussed above remains to be investigated in future experiments. It is likely, however, that surface plasmons also play a decisive role in the case of ion desorption since their kinetic energies decrease for excitation at the plasmon frequency[50] (see also Fig. 12).

The observation of laser desorption of a variety of metal atoms, i.e., Na, K, Au, Ag, and Al from clusters as well as from thin metal films indicates the general nature of the desorption process. As described in the present paper, metal clusters have the advantage that they can serve as model systems for the investigation of the mechanism of metal-atom desorption in general. Their size can be varied in a well-defined manner which changes the number of sites from which desorption occurs, and changes the electric-field enhancement in the surface region. Under such conditions, the process is understood more easily than by experiments on rough films that are difficult to characterize. In future experiments, it will be interesting to study how the desorption rate changes if the metal particles increase in size and grow together, finally forming a continuous film. Another interesting question is whether desorption can also be detected for excitation with frequencies far outside the surface plasmon resonance. Since there would be no meaningful field enhancement, high-power pulsed laser light is required. Such experiments are currently under preparation in our laboratory. In further work the repulsive single-electron state from which desorption takes place will also have to be characterized in more detail.

ACKNOWLEDGMENT

Financial support of the Deutsche Forschungsgemeinschaft is gratefully acknowledged.

[1]The notations "particle" and "cluster" will be used synonymously throughout this paper.

[2]W. Hoheisel, K. Jungmann, M. Vollmer, R. Weidenauer, and F. Träger, Phys. Rev. Lett. **60**, 1649 (1988).

[3]W. Hoheisel, U. Schulte, M. Vollmer, R. Weidenauer, and F. Träger, Appl. Surf. Sci. **36**, 664 (1989).

[4]W. Hoheisel, U. Schulte, M. Vollmer, and F. Träger, Appl. Phys. A **51**, 271 (1990).

[5]W. Hoheisel, M. Vollmer, and F. Träger, Appl. Phys. A **52**, 445 (1991).

[6]A. M. Bonch-Bruevich, Yu. N. Maksimov, S. G. Przhibel'skii, and V. V. Khromov, Zh. Eksp. Teor. Fiz. **92**, 285 (1987) [Sov. Phys. JETP **65**, 161 (1987)].

[7]A. M. Bonch-Bruevich, T. A. Vartanyan, Yu. N. Maksimov, S. G. Przhibel'skii, and V. V. Khromov, Zh. Eksp. Teor. Fiz. **97**, 1761 (1990) [Sov. Phys. JETP **70**, 993 (1990)].

[8]I. Lee, J. E. Parks II, T. A. Callcott, and E. T. Arakawa, Phys. Rev. B **39**, 8012 (1989).

[9]E. T. Arakawa, I. Lee, and T. A. Callcott, in *Laser Ablation—Mechanisms and Applications,* edited by J. C. Miller and R. F. Haglund, Jr., Springer Lecture Notes in Physics Vol. 389 (Springer, Berlin, 1991), p. 82.

[10]M. J. Shea and R. N. Compton, in *Laser Ablation—Mechanisms and Applications* (Ref. 9), p. 234.

[11]R. H. Ritchie, J. R. Manson, and P. M. Echenique, in *Laser Ablation—Mechanisms and Applications* (Ref. 9), p. 234.

[12]*Desorption Induced by Electronic Transitions, DIET IV,* edited by G. Betz and P. Varga, Springer Series in Surface Science Vol. 19 (Springer, Berlin, 1990).

[13]D. Menzel and R. Gomer, J. Chem. Phys. **41**, 3311 (1964).

[14]P. A. Readhead, Can. J. Phys. **42**, 886 (1964).

[15]M. L. Knotek and P. J. Feibelmann, Phys. Rev. Lett. **40**, 964 (1978).

[16]T. J. Chuang, Surf. Sci. Rep. **3**, 1 (1983).

[17]W. Ho, Comm. Condens. Matter Phys. **13**, 293 (1988).

[18]F. Träger, in *Photoacoustic, Photothermal and Photochemical Processes at Surfaces and in Thin Films,* edited by P. Hess, Topics in Current Physics Vol. 47 (Springer, Berlin, 1989).

[19]R. Monreal and A. P. Apell, Phys. Rev. B **41**, 7852 (1990).

[20]M. Vollmer and F. Träger, Z. Phys. D **3**, 291 (1986).

[21]M. Vollmer and F. Träger, Surf. Sci. **187**, 445 (1987).

[22]T. Götz, W. Hoheisel, M. Vollmer, and F. Träger (unpublished); T. Götz, M. Vollmer, and F. Träger, Appl. Phys. A **57**, 101 (1993).

[23]ND_3 can be detected with a lower background counting rate by the mass spectrometer as compared to NH_3.

[24]M. Vollmer, R. Weidenauer, W. Hoheisel, U. Schulte, and F. Träger, Phys. Rev. B **40**, 12 509 (1989).

[25]K. Höning, W. Hoheisel, M. Vollmer, and F. Träger (unpublished).

[26]In an earlier paper (Ref. 2) a value of 1.64 eV for the kinetic energy was quoted. It resulted from an incorrect value for the drift time of the ions in the quadrupole mass spectrometer.
[27]Previously published spectra of K particles [J.-C. Payan and D. Roux, Opt. Comm. **7**, 26 (1973)] exhibit a maximum at a wavelength above 1000 nm, a range presently not accessible in our experiment.
[28]G. Mie, Ann. Phys. **25**, 377 (1908).
[29]U. Kreibig and L. Genzel, Surf. Sci. **156**, 678 (1985).
[30]M. Vollmer and U. Kreibig, in *Nuclear Physics Concepts in the Study of Atomic Cluster Physics,* edited by R. Schmidt, H. O. Lutz, and R. Dreizler, Springer Lecture Notes in Physics Vol. 404 (Springer, Berlin, 1992), p. 266.
[31]M. Vollmer and U. Kreibig, Optical Properties of Metal Clusters (Springer, Berlin, in press).
[32]C. F. Bohren and D. R. Huffman, *Absorption and Scattering of Light by Small Particles* (Wiley, New York, 1983).
[33]H. Poppa, J. Vac. Sci. Technol. **2**, 42 (1965).
[34]H. Schmeisser, Thin Solid Films **22**, 83 (1974).
[35]T. Inagaki, L. C. Emerson, E. T. Arakawa, and M. W. Williams, Phys. Rev. B **13**, 2305 (1976).
[36]N. V. Smith, Phys. Rev. **183**, 634 (1969).
[37]Å. Ljungbert and S. Lundqvist, Surf. Sci. **156**, 839 (1985).
[38]P. Feibelmann, Prog. Surf. Sci. **12**, 287 (1982).
[39]H. J. Levinson, E. W. Plummer, and P. J. Feibelman, Phys. Rev. Lett. **43**, 952 (1979).
[40]N. D. Lang and W. Kohn, Phys. Rev. B **1**, 4555 (1970).
[41]W. Ekardt, Phys. Rev. B **29**, 1558 (1984).
[42]P. Apell and Å. Ljungbert, Phys. Scr. **26**, 113 (1982).
[43]P. Apell and Å. Ljungbert, Solid State Commun. **44**, 1367 (1982).
[44]P. Apell and D. R. Penn, Phys. Rev. Lett. **50**, 1316 (1983).
[45]P. Apell, J. Giraldo, and S. Lundqvist, Phase Trans. **24-26**, 577 (1990).
[46]To our knowledge no calculation, including all retardation effects, has been performed so far for this nonlocal approach.
[47]A. Liebsch, Phys. Rev. B **36**, 7378 (1987).
[48]In this size range the electric-field enhancement is almost constant ($\lambda = 510$ nm).
[49]B. J. Messinger, K. U. von Raben, R. K. Chang, and P. W. Barber, Phys. Rev. B **24**, 649 (1981).
[50]H. Helvajian (private communication) and (unpublished).
[51]H. Helvajian and R. Welle, J. Chem. Phys. **91**, 2616 (1989); H. S. Kim and H. Helvajian, *ibid.* **95**, 6623 (1991).